water

MDPI

Article

Enhanced Degradation of Deltamethrin in Water through Ferrous Ion Activated Sulfite: Efficiency and Mechanistic Insights

Ying Wan [1,2,3,†], Fangze Shang [1,†], Luming Yin [2], Hantao Wang [1], Yang Ping [1], Jiaqi Ding [2,3,*], Zongping Wang [2,*] and Pengchao Xie [2]

[1] Power China Eco-Environmental Group Co., Ltd., Shenzhen 518101, China; wanying@hust.edu.cn (Y.W.); shangfz-shj@powerchina.cn (F.S.); wanghant-shj@powerchina.cn (H.W.); pingyang-shj@powerchina.cn (Y.P.)
[2] School of Environmental Science and Engineering, Huazhong University of Science and Technology, Wuhan 430074, China; 15527589179@163.com (L.Y.); pengchao.x@gmail.com (P.X.)
[3] Changjiang Basin Ecology and Environment Monitoring and Scientific Research Center, Changjiang Basin Ecology and Environment Administration, Ministry of Ecology and Environment, Wuhan 430010, China
* Correspondence: dingjiaqi_1993@163.com (J.D.); zongpingw@hust.edu.cn (Z.W.)
† These two authors contributed equally to this work.

Abstract: Deltamethrin's global use as a potent insecticide against pests is well-established. However, the compound's diverse levels of toxicity are increasingly under scrutiny, drawing significant attention to treatments of deltamethrin. Transition metal activation of sulfite is a promising technology for micropollutant degradation. In this study, iron-activated sulfite was used for the degradation of deltamethrin. The degradation effects and influencing factors and the underlying mechanism of deltamethrin degradation in the system were investigated. The degradation of deltamethrin was effectively achieved by the Fe (III)/sulfite system. The optimal reaction conditions at laboratory scale were determined to be an initial pH of 4, a Fe (III) concentration of 100 μM, and a HSO_3^- concentration of 1 mM, where the degradation rate was approximately 69.5%. Dissolved oxygen was identified as an essential factor in the reaction process, with the degradation rate of deltamethrin decreasing by up to 22% under anaerobic conditions. The presence of light facilitated the degradation of deltamethrin within the reaction system, while bicarbonate and natural organic compounds were found to inhibit its degradation. Quenching experiments verified the presence of hydroxyl radicals ($HO^•$) and sulfate radicals ($SO_4^{•-}$) in the reaction system, with $HO^•$ being the predominant species. This was further confirmed by EPR experiments. Additionally, density functional theory calculations indicated the propensity for bond breaking between C16 and O21 in deltamethrin molecules, and the degradation pathway was validated through GC-MS analysis of the products formed. Moreover, the Fe (III)/sulfite system demonstrated good degradation performance for deltamethrin in secondary effluent, achieving degradation rates of 46.3%. In particular, the Fe (III)/sulfite system showed minimal bromate formation, attributed to the capacity of sulfite to reduce active bromine intermediates into bromine ions.

Keywords: deltamethrin; ferric ion; sulfite; sulfate radical ($SO_4^{•-}$); density functional theory

Citation: Wan, Y.; Shang, F.; Yin, L.; Wang, H.; Ping, Y.; Ding, J.; Wang, Z.; Xie, P. Enhanced Degradation of Deltamethrin in Water through Ferrous Ion Activated Sulfite: Efficiency and Mechanistic Insights. *Water* **2024**, *16*, 8. https://doi.org/10.3390/w16010008

Academic Editor: Carmen Teodosiu

Received: 14 November 2023
Revised: 12 December 2023
Accepted: 15 December 2023
Published: 19 December 2023

1. Introduction

Synthetic pyrethroids (SPs) are among the most widely used pesticides in the world, and the application of them has increased significantly in recent decades due to their efficacy and low toxicity compared to other pesticides [1]. Deltamethrin ((S)-alpha-cyano-3-phenoxybenzyl-(1R)-cis-3-(2,2-dibromovinyl)-2,2-dimethylcyclopropane carboxylate), a type II synthetic pyrethroid, has made significant contributions to global agricultural development [2]. However, the extensive usage of deltamethrin has led to significant increased concentrations of pesticides in the soil and water, which can enter the food chain, posing potential threats to human health, food safety, and the ecological environment [1,3]. Toxicokinetic studies of deltamethrin and its metabolites have shown that accumulation of

deltamethrin and its metabolites increases neurotoxicity and that it is significantly toxic to vertebrates and invertebrates [3]. Currently, research on deltamethrin removal from the environment has gained considerable attention [4,5].

Sulfate radicals-based advanced oxidation technologies (SR-AOPs) have demonstrated exceptional efficacy in the removal of organic pollutants [6,7]. The production method of $SO_4^{\bullet-}$ is mainly based on the activation of persulfate [8]. However, practical water treatment applications encounter challenges associated with persulfate, such as high expense and potential toxicity [9,10]. Sulfite, a byproduct of flue gas desulfurization, presents a cost-effective and environmentally friendly alternative. After activation, it generates various active free radicals, including hydroxyl radicals ($HO^{\bullet}$) and sulfate radicals ($SO_4^{\bullet-}$) [10–12]. In recent years, sulfite has garnered recognition as a promising substitute for persulfate, progressively gaining prominence in the area of pollutant treatment [13,14].

At present, a variety of methods and chemicals have been employed to activate sulfite and generate $SO_4^{\bullet-}$, including ultraviolet radiation, low-valence transition metals such as Fe(II) and Cu(II), oxidizing agents like potassium permanganate and potassium ferrate, and heterogeneous materials such as zero-valent iron [15–17]. Notably, there is growing interest in SR-AOPs based on the activation of bisulfite by transition metals [18]. Among the different transition metals, Fe was considered to be an excellent activator for sulfite due to its abundance, cost-effectiveness, and non-toxic nature [19]. The mechanisms underlying the activation of sulfite by transition elements can be categorized into two primary types. The first theory involves non-free radicals. Taking Fe(III) as an example, it combines with sulfite and absorbs an oxygen molecule, which then decomposes into sulfite and Fe(II). In contrast, the free radical theory suggests that during the reaction process, sulfite directly donates an electron to generate the sulfate radical.

The reaction process can be elucidated through Equations (1)–(12) in Table 1 [20–26]. Initially, Fe (III) reacts with HSO_3^- to form $FeSO_3^+$, subsequently yielding $SO_3^{\bullet-}$ [27]. The rate-limiting step in the overall reaction happens during the reduction of Fe (III) to Fe (II). Following this, $SO_3^{\bullet-}$ undergoes oxidation by O_2 to generate $SO_5^{\bullet-}$, with a portion of $SO_5^{\bullet-}$ participating in further reactions, producing SO_5^-, and the other part generating $S_2O_8^-$ [28,29]. Subsequently, $S_2O_8^-$ is activated by Fe (II) to form $SO_4^{\bullet-}$, which, in turn, undergoes oxidation to regenerate Fe (III). This cyclic process ensures the continuous involvement of Fe throughout the reaction [19,30].

Table 1. The potential reactions in Fe(III)/sulfite process.

$Fe^{2+} + HSO_3^- \rightleftharpoons FeHSO_3^+ (\log\ k = 4)$	(1)
$4FeHSO_3^+ + O_2 \rightarrow 4FeSO_3^+ + 2H_2O\ k = 1.69 \times 10^3\ M^{-1}s^{-1}$	(2)
$Fe^{3+} + HSO_3^- \rightleftharpoons FeSO_3^+ + H^+ (\log\ k = 2.45)$	(3)
$FeSO_3^+ \rightarrow Fe^{2+} + SO_3^{\bullet-} k = 0.19\ s^{-1}$	(4)
$SO_3^{\bullet-} + O_2 \rightarrow SO_5^{\bullet-} k = (1.1 - 2.5) \times 10^9\ M^{-1}s^{-1}$	(5)
$SO_5^{\bullet-} + HSO_3^- \rightarrow SO_4^{2-} + SO_4^{\bullet-} + H^+ k \approx 1.2 \times 10^4\ M^{-1}s^{-1}$	(6)
$SO_5^{\bullet-} + HSO_3^- \rightarrow HSO_5^- + SO_3^{\bullet-} k < 3 \times 10^5\ M^{-1}s^{-1}$	(7)
$SO_5^{\bullet-} + SO_5^{\bullet-} \rightarrow 2SO_4^{\bullet-} + O_2\ k = 10^6 - 10^8\ M^{-1}s^{-1}$	(8)
$SO_5^{\bullet-} + SO_5^{\bullet-} \rightarrow S_2O_8^{2-} + O_2\ k = 10^7 - 10^8\ M^{-1}s^{-1}$	(9)
$Fe^{2+} + S_2O_8^{2-} \rightarrow Fe^{3+} + SO_4^{\bullet-} + SO_4^{2-}\ k = 20\ M^{-1}s^{-1}$	(10)
$SO_4^{\bullet-} + HSO_3^- \rightarrow SO_4^{2-} + SO_3^{\bullet-} + H^+ k = 1.3 \times 10^8 - 2.5 \times 10^9\ M^{-1}s^{-1}$	(11)
$Fe^{2+} + HSO_3^- \rightarrow Fe^{3+} + SO_4^{\bullet-} + OH^-\ k = 10^4 - 10^7\ M^{-1}s^{-1}$	(12)

In a study by Chen et al., the degradation of Orange II was compared by activating sulfites with Fe(II) and Fe(III). Interestingly, the Fe(III) system exhibited a slightly faster reaction rate than the Fe(II) system [20]. This disparity can be attributed to the fact that $FeSO_3^+$ can directly participate in the reaction process, whereas $FeHSO_3^+$ necessitates oxidation to become $FeSO_3^+$ before it can contribute to the reaction. The comparable reaction rates between the Fe(III) and Fe(II) systems indicate that the conversion reaction time from $FeHSO_3^+$ to $FeSO_3^+$ was extremely short, and Equation (4) is the true rate-limiting step in

the reaction process. Zhang et al. introduced xenon lamp illumination into the reaction system, building upon Chen's research, and observed that xenon lamp irradiation enhanced the degradation of Orange II while expanding the optimal pH range of the system [31]. The intricate free radical conversion reactions inherent in sulfite AOPs frequently lead to debates regarding the reaction mechanism within the same sulfite AOP framework [30,32]. Currently, the sulfite auto-oxidation system is still in its nascent stages of development. It holds promise as a cost-effective and efficient advanced oxidation technology with the theoretical capability to effectively degrade pyrethroids. However, the research in this field is currently limited, with insufficient understanding regarding the impact of various factors on pollutant degradation and identification of active species within sulfite auto-oxidation systems. Furthermore, it has been reported that bromate was easily formed in traditional advanced oxidation processes in the presence of Br^-. Due to the relative weak oxidative properties of sulfite, the potential control of bromate formation in a sulfite auto-oxidation system requires further investigation.

The primary objectives of this study are (1) to conduct a comparative analysis of deltamethrin degradation by various systems, including Fe^0/sulfite, Fe(II)/sulfite, Fe(III)/sulfite, Fe_2O_3/sulfite, and Fe_3O_4/sulfite, with the aim of identifying the most suitable reaction system for efficient deltamethrin degradation; (2) to investigate the impact of diverse influencing factors on the degradation efficiency of deltamethrin within the identified optimal system; (3) to elucidate the active substances responsible for deltamethrin degradation within the optimal system and unveil the associated degradation mechanism; (4) to assess the removal efficiency of the Fe (III)/sulfite system on pollutants present in the effluent of real-world secondary sedimentation tanks, thereby evaluating the engineering feasibility and practicality of this system; and (5) to evaluate the formation of bromate in the presence of Br^-.

2. Material and Methods

2.1. Materials

Deltamethrin ($C_{22}H_{19}Br_2NO3$, 52918-63-5) was procured from Aladdin Reagent Company (Shanghai, China). Sodium sulfite (Na_2SO_3, 7757-83-7), iron sulfate ($Fe_2(SO_4)_3$, 10028-22-5), ferrous sulfate ($FeSO_4$, 7720-78-7), iron oxide (Fe_2O_3, 1332-37-2), ferric oxide (Fe_3O_4, 12227-89-3), elemental iron (Fe, 7439-89-6), sodium hydroxide (NaOH, 1310-73-2), sulfuric acid (H_2SO_4, 7664-93-9), sodium bicarbonate ($NaHCO_3$, 144-55-8), and humic acid (HA, 308067-45-0) were obtained from China National Pharmaceutical Group Chemical Reagent Co., Ltd (Shanghai, China). Tert-butanol (TBA, 75-65-0), methanol (MeOH, 170082-17-4), and ethanol (EtOH, 64-17-5) were acquired from Tedia Chromatographic Reagent Company (Fairfield, CT, USA). Sodium thiosulfate ($Na_2S_2O_6$, 7772-98-7), phenanthroline ($C_{12}H_8N_2 \cdot H_2O$, 66-71-7), hydroxylamine hydrochloride ($HONH_3Cl$, 5470-11-1), acetic acid ($C_2H_4O_2$, 64-19-7), ammonium acetate ($C_2H_7O_2N$, 631-61-8), sodium sulfate (Na_2SO_4, 7757-82-6), and sodium bromide (NaBr, 7647-15-6) were also sourced from China National Pharmaceutical Group Chemical Reagent Co., Ltd (Shanghai, China). The secondary effluent, sourced from a wastewater treatment plant in Wuhan, was collected and transferred to the laboratory. The water samples underwent filtration using a 0.45 μm membrane and were subsequently stored at 4 °C, shielded from light exposure.

2.2. Experimental Procedure

Throughout the experiment, ultrapure water (250 mL) was accurately measured and placed in a 250 mL volumetric flask, followed by a 15 min preheating in a constant-temperature water bath set at 25 °C. Subsequently, the preheated solution was transferred to a beaker or conical flask reactor. The activation of a magnetic stirrer was initiated at a speed of 400 r/min, and pH monitoring was conducted within the reactor using a pH meter. Sequentially, a specified volume of deltamethrin solution and iron sulfate stock solution were introduced into the reactor, followed by the addition of sodium sulfite to initiate the reaction, with timing initiated concurrently. The initial pH stability of the

reaction solution was maintained at 4.0 ± 0.2 using a 0.1 M dilute sulfuric acid and 0.1 M sodium hydroxide solution. Fe(II) in the Fe(II)/sulfite system was derived from a $FeSO_4$ stock solution, and Fe(III) in the Fe(III)/sulfite system was derived from a $Fe_2(SO_4)_3$ stock solution. The reaction vessel was shielded using tin foil to explore the influence of light. A xenon lamp (PL-X300D, Pulinsaisi, Beijing, China) was employed to simulate sunlight conditions in the experimental setup, and the incident light intensity was measured and described in Test S1 in the Supplementary Materials.

Sampling occurred at specified intervals of 0, 1, 3, 5, 10, 20, and 30 min. During the sampling process, 10 mL of the upper reaction solution was aspirated using a pipette and transferred into a 20 mL brown extraction bottle. To quench the reaction, 200 µL of sodium thiosulfate stock solution was introduced into the extraction bottle. Following this, 2 mL of petroleum ether and 4.0 g of anhydrous sodium sulfate were incorporated, and vigorous shaking was performed using a vortex oscillator for three minutes. During the shaking procedure, the bottle cap was intermittently opened to release gas, and subsequently, the mixture was allowed to stand for 10 min. Approximately 1 mL of the upper organic phase was withdrawn and deposited into a 2 mL brown gas-phase vial for subsequent analysis and determination. Each experimental group underwent a minimum of two trials, with the average value serving as the basis for result analysis.

2.3. Analysis

Deltamethrin was determined using a Shimadzu GC-2014C gas chromatograph (equipped with an ECD detector). During the detection process, the injection port temperature was set at 280 °C, the detector temperature was set at 300 °C, and the chromatographic column was a DB-5MS column (30 m × 0.25 µm × 0.25 µm). The temperature program of the oven began at 80 °C for 1 min and was then ramped up to 280 °C at a rate of 40 °C/min and held for 6 min.

Fe (II)/Fe (III) and total iron concentration were detected using the o-phenanthroline method. Electron paramagnetic resonance spectroscopy (EPR) detection and chemical reagent quenching were used to identify the primary free radical species involved in the reaction processes. The GC-MS carried out with a HP-5MS chromatographic column (30 m × 0.25 µm × 0.25 µm) was used for the analysis of degradation products. The carrier gas is high-purity He gas (>99.999%), with a flow rate of 1 mL/min and a sample inlet temperature of 220 °C. The temperature program of the oven began at 35 °C for 0 min, increased to 240 °C at a rate of 8 °C/min, and held for 22 min. Br^- and BrO_{3^-} were determined using ion chromatography with a $Na_2CO_3/NaHCO_3$ buffer as the mobile phase and a flow rate of 1 mL/min [33]. Chemical oxygen demand (COD), ammonia nitrogen (NH_3-N), and total phosphorus (TP) were analyzed by potassium dichromate digestion, Nessler reagent colorimetry, and ammonium molybdate spectrophotometry, respectively (China-EPA, 2002) [34]. pH and turbidity were measured by a pH meter (Starter-3100, Ohaus, Parsippany, NJ, USA) and a turbidity meter (WGZ-2, Ruixin, Shanghai, China), respectively.

The determination of active sites within the deltamethrin molecules was performed using Gaussian09 software. Calculations were carried out at the B3LYP level, employing the 6-31 + G (d, p) basis set. Subsequently, optimized natural space orbit analysis, also known as NBO charge calculation, was conducted on deltamethrin molecules to pinpoint their active sites. The Fukui function, a crucial parameter within density functional theory, provides a direct numerical reflection of active sites during the reaction process. The calculation formula for the Fukui function is shown in Equation (13) [35].

$$f_k^0 = \frac{(q_k^{N-1} - q_k^{N+1})}{2} \quad (13)$$

where, the f_k^0 is the Fukui function value, k represents the atomic number in deltamethrin, N represents the number of electrons outside the nucleus, and q_k is the charge symbol.

3. Results and Discussion

3.1. Degradation of Deltamethrin by Fe(III)-Activated Systems

3.1.1. Comparison of Deltamethrin Degradation in Different Systems

The results of deltamethrin degradation in different systems are shown in Figure 1. It can be seen that Fe(III)/sulfite, Fe(II)/sulfite, and Fe^0/sulfite systems all exhibited commendable performance in the degradation of deltamethrin. Notably, both the Fe(III)/sulfite and Fe(II)/sulfite systems achieved a degradation rate of 69.5% after 30 min. During the initial 20 min of the reaction, the degradation rate of the Fe(III)/sulfite system was slightly higher than that of the Fe(II)/sulfite system, which is consistent with the findings of Chen et al. [20]. Consequently, the Fe(III)/sulfite system was determined as the main experimental condition for the reaction. The Fe^0/sulfite system also demonstrated relatively efficient degradation, which can be attributed to the photocatalytic reaction occurring on the surface of Fe^0 in the presence of O_2 [36]. During these reaction processes, as seen in Equations (14)–(16), Fe(II) and Fe(III) could be formed, initiating the sulfur auto-oxidation system reaction [37].

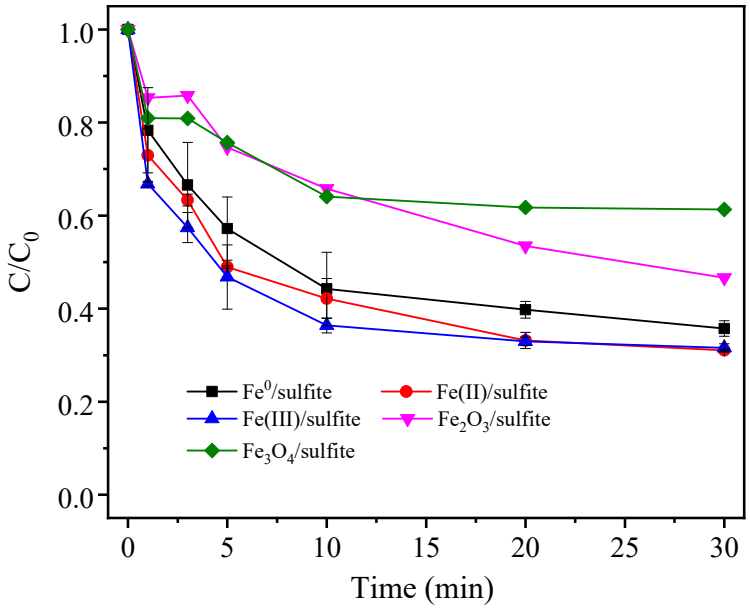

Figure 1. The degradation of deltamethrin by different reaction systems. Condition: $[Deltamethrin]_0$ = 30 μg/L, $[Fe(III)]_0 = [Fe(II)]_0 = [Fe(0)]_0 = 2[Fe_2O_3]_0 = 3[Fe_3O_4]_0$ = 100 μM, $[HSO_3^-]_0$ = 1 mM, $pH_0 = 4.0 \pm 0.2$, temperature = 25 °C. The error bars represent the standard deviations.

A portion of deltamethrin could also be removed by Fe_2O_3/sulfite and Fe_3O_4/sulfite systems, which can be attributed to the generation of Fe(III) and Fe(II). On the one hand, Fe_2O_3 and Fe_3O_4 can gradually react with H^+ to produce Fe(III) and Fe(II) with the initial reaction pH of 4.0. On the other hand, Fe_2O_3 and Fe_3O_4 can undergo oxidation reactions with sulfite, which results in the gradual release of Fe(III) and Fe(II) into the aqueous solution. The degradation efficiency achieved by the Fe_2O_3/sulfite and Fe_3O_4/sulfite systems displayed a similar tendency during the first 10 min of reaction, but a difference emerged in the degradation rate during the period from 10 to 30 min. This variation may be attributed to the consumption of free radicals by Fe(II) generated from Fe_3O_4, leading to a relatively lower degradation efficiency compared to Fe_2O_3. Additionally, previous studies have also reported that the reaction rate between Fe_3O_4 and sulfite was lower than that between Fe_2O_3 and sulfite in aqueous solutions, which may provide another explanation for the inhibited degradation of deltamethrin by the Fe_3O_4/sulfite system [38].

$$Fe^0 + O_2 + 2H^+ \rightarrow Fe(II) + H_2O_2 \quad (14)$$

$$Fe^0 + H_2O_2 + 2H^+ \rightarrow Fe(II) + 2H_2O \quad (15)$$

$$Fe(II) + H_2O_2 \rightarrow Fe(III) + OH^- + HO^\bullet \quad (16)$$

3.1.2. Changes of Fe(III)/Fe(II) and Sulfite Species during the Reaction Process

As depicted in Figure 2a, an excess of sulfite led to the rapid reduction of Fe(III) to Fe(II) within the initial 15 s. As the reaction prolonged, Fe(II) was oxidized by sulfite to $FeSO_3^+$ in the presence of abundant O_2. The conversion from Fe(II) to Fe(III) was quick and finished after a reaction of approximately 5 min. As shown in Figure 2b, the concentration of sulfite continuously decreased with prolonged reaction, which was consumed completely after a reaction of about 20 min. This is attributed to the fact that Equation (4) is the rate-limiting step of the chain reaction. The consumption tendency of sulfite was similar to the degradation process of deltamethrin, which demonstrated that the concentration of sulfite was the key influencing factor during the reaction process.

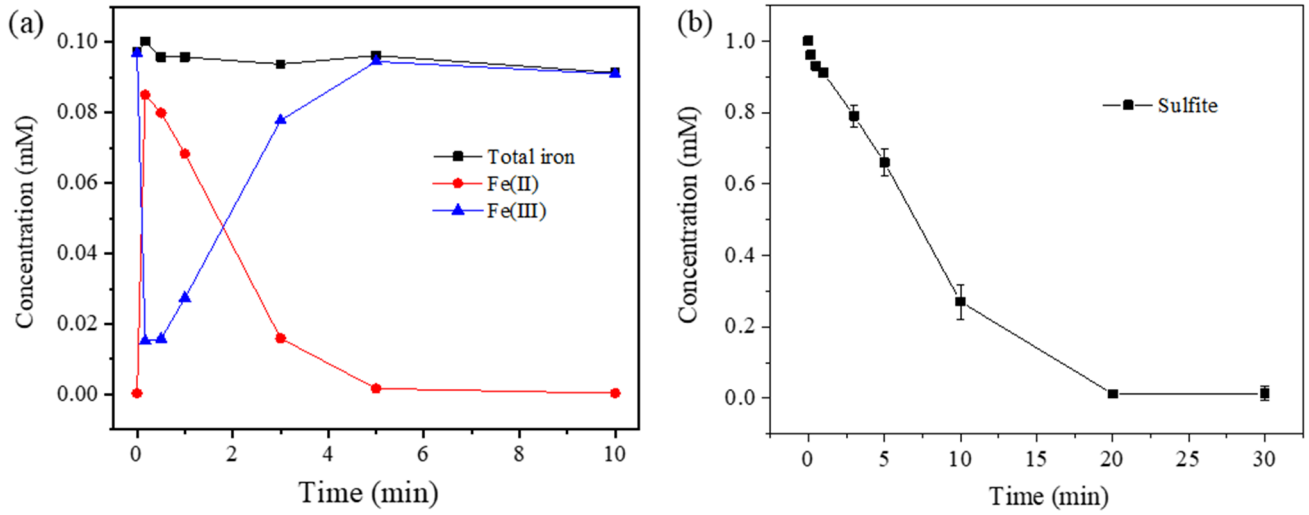

Figure 2. The change of iron species during the reaction (**a**) and the consumption of sulfite during the reaction (**b**). Condition: $[Deltamethrin]_0$ = 30 μg/L, $[Fe(III)]_0 = [Fe(II)]_0 = [Fe(0)]_0 = 2[Fe_2O_3]_0 = 3[Fe_3O_4]_0$ = 100 μM, $[HSO_3^-]_0$ = 1 mM, pH_0 = 4.0 ± 0.2, temperature = 25 °C. The error bars represent the standard deviations.

3.2. Effect of Initial pH

The pH value plays a significant role in determining the form of iron ions and sulfite in the reaction system, thereby affecting the degradation of deltamethrin by Fe(III)/sulfite system. In consideration of the reported self-decomposition of deltamethrin in an alkaline solution [39], the impact of initial pH values ranging from 3.0 to 7.0 on deltamethrin degradation in the Fe(III)/sulfite system were evaluated. As shown in Figure 3a, the degradation of deltamethrin decreased from 76.5% to 38.1% after a 30 min reaction as the reaction pH increased from 3.0 to 7.0. Additionally, the reaction pH was also monitored during the reaction in the system (Figure 3b). With the progression of the oxidation process, the chosen pH (4.0, 5.0 and 6.0) swiftly decreased and eventually stabilized at around 3.5–4.0. In contrast, the pH remained stable at pH 3.0. As reported in previous studies [40,41], HSO_3^- is the dominant species of sulfite in the pH range of 3.0–6.0, which is conducive to the generation of $FeSO_3^+$. Furthermore, HSO_3^- is an essential component in reaction Equation (12), promoting the generation of $SO_4^{\bullet-}$ and improving the reaction rate. However, as the pH gradually increased from 3 to 7, HSO_3^- was gradually transformed into SO_3^{2-}, inhibiting the generation of free radicals and exerting a suppressive effect on the degradation of deltamethrin.

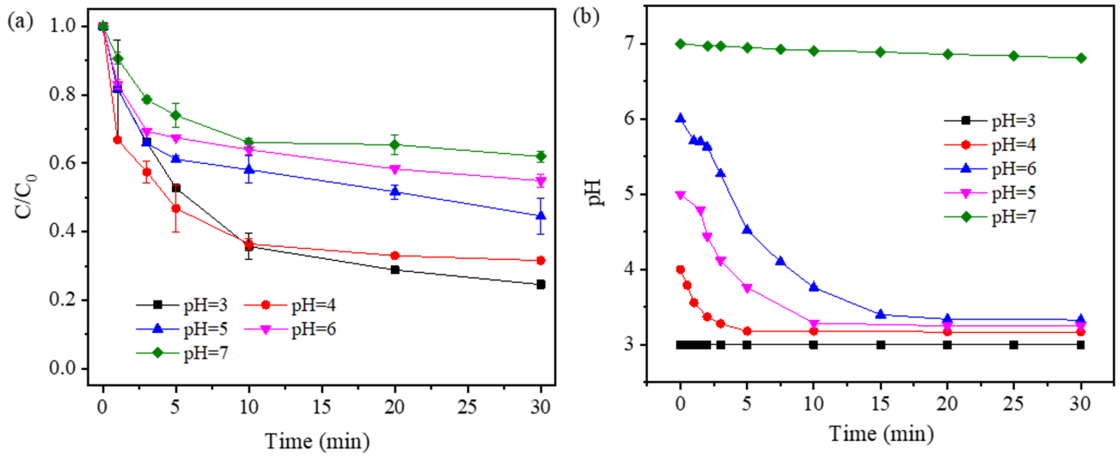

Figure 3. Effect of initial pHs on deltamethrin removal in the Fe(III)/sulfite system (**a**) and the variation of solution pH during the degradation of deltamethrin (**b**). Condition: $[Deltamethrin]_0$ = 30 μg/L, $[Fe(III)]_0$ = 100 μM, $[HSO_3^-]_0$ = 1 mM, temperature = 25 °C. The error bars represent the standard deviations.

3.3. Effect of Initial Fe(III) Concentration, Initial Sulfite Concentration on Deltamethrin Removal

The effects of initial Fe(III) concentration and initial sulfite concentration on deltamethrin degradation within the Fe(III)/sulfite system were also studied, as illustrated in Figures 4a and 4b, respectively. Figure 4a shows the effect of Fe(III) concentration ranging from 60 to 150 μM on the degradation of deltamethrin (30 μg/L) with an initial sulfite concentration of 1.0 mM. The removal efficiency of deltamethrin increased from 58.0% to 69.5% after a 30 min reaction, while the initial Fe(III) concentration increased from 60 to 100 μM. However, the removal of deltamethrin slightly decreased, while the Fe(III) concentration was further raised to 120 and 150 μM. This result suggests that the optimal concentration of Fe(III) under these conditions is approximately 100 μM, which is consistent with the optimal ratio of Fe(III) to sulfite (1:10) reported in previous studies [31]. When the Fe(III) concentration exceeds the optimal level, superfluous Fe(III) can consume part of the sulfite, which inhibits the degradation of deltamethrin [42].

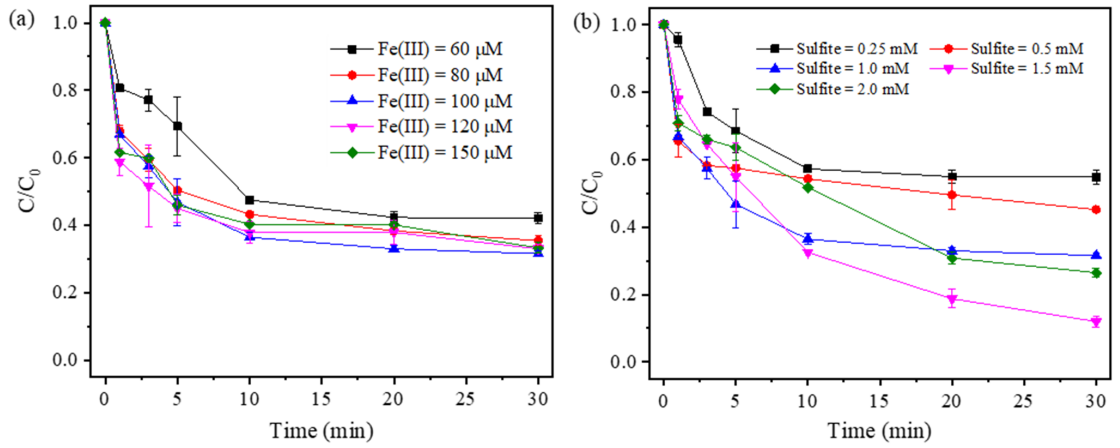

Figure 4. Effect of (**a**) initial Fe(III) concentration and (**b**) initial sulfite concentration on deltamethrin removal in the Fe(III)/HSO_3^- system. Condition: $[Deltamethrin_0]$ = 30 μg/L, $[HSO_3^-]_0$ = 1 mM for (**a**), $[Fe(III)]_0$ = 100 μM for (**b**), pH_0 = 4.0 ± 0.2, temperature = 25 °C. The error bars represent the standard deviations.

Figure 4b shows the effect of sulfite concentration ranging from 0.25 to 2 mM on the degradation of deltamethrin (30 μg/L) with an initial Fe(III) concentration of 100 μM. After

a 30 min reaction, the degradation rate of deltamethrin increased from 45.2% to 88.0% as the sulfite concentration increased from 0.25 to 1.5 mM. However, it decreased to 73.5% with the further increase of sulfite to 2.0 mM. This trend aligns with previous findings [42,43]. The increase of sulfite mainly contributes to the stimulation process for the generation of $FeSO_3^+$ and $SO_4^{\bullet -}$, which promote the degradation of deltamethrin. However, sulfite can also react with $SO_4^{\bullet -}$ with a high reaction rate. Equation (11) shows competition with deltamethrin for free radicals while excessive sulfite is present in the system.

3.4. Effect of HCO_3^-, HA, Dissolved Oxygen and Photo Radiation on Deltamethrin Removal

The effects of HCO_3^- and HA on the degradation of deltamethrin are shown in Figure 5a,b. It can be seen that HCO_3^- and HA significantly restrain the removal of deltamethrin in the Fe(III)/sulfite system, which is consistent with the conclusion reached in other researches [44,45]. The degradation rate of deltamethrin decreased from 69.5% to 33.1% as the HCO_3^- concentration increased from 0 to 1 mM. When the HA concentration increased to 10 mg/L, the degradation of deltamethrin after a 30 min reaction was reduced by 45%. Both HCO_3^- and HA are common scavengers for reactive radicals, which shows competition with deltamethrin for free radicals. HCO_3^- shows a good buffering capacity, which hinders the decrease of pH during the reaction process (as shown in Figure S1, Supplementary Materials), leading to partial sedimentation of Fe(III) and a decrease in degradation efficiency of deltamethrin.

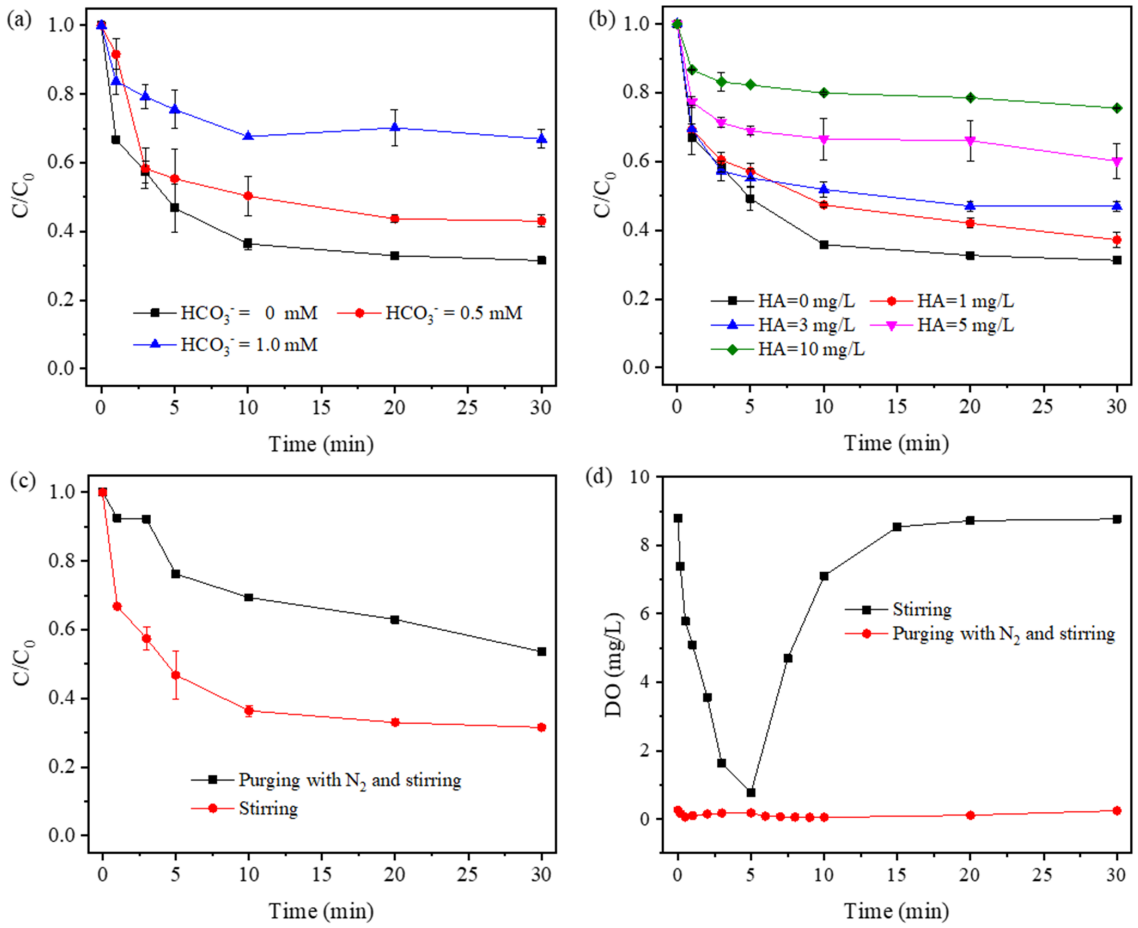

Figure 5. (**a**) the effect of HCO_3^- on the degradation of deltamethrin, (**b**) the effect of HCO_3^- on the degradation of deltamethrin HA, (**c**) the effect of dissolved oxygen on the degradation of deltamethrin, and (**d**) changes in dissolved oxygen during the degradation of deltamethrin. Condition: $[Deltamethrin]_0$ = 30 μg/L, $[Fe(III)]_0$ = 100 μM, $[HSO_3^-]_0$ = 1 mM, pH = 4 ± 0.2. The error bars represent the standard deviations.

Dissolved oxygen also plays a crucial role in the Fe(III)/sulfite system, as it participates in reactions (2) and (5), promoting the generation of reactive oxygen species such as $O_2^{\bullet-}$ and $HO^{\bullet}$ [46]. In this experiment, the degradation of deltamethrin under anaerobic conditions was investigated by continuously purging the reaction system with N_2, as shown in Figure 5c. A comparison experiment between N_2 purging and continuous stirring revealed a significant difference in the degradation efficiency of deltamethrin. Under N_2 purging conditions, the degradation efficiency decreased by 22.0%. Additionally, by observing the changes in dissolved oxygen under only stirring conditions in Figure 5d, it can be seen that within the initial 5 min of the reaction, the dissolved oxygen in the reaction system rapidly decreased to 0.778 mg/L. This highlights the essential nature of dissolved oxygen during this phase of the reaction, aligning with the degradation curve where the majority of deltamethrin degradation occurs within the first 5 min. As the reaction progresses, the dissolved oxygen in the reaction system is gradually consumed, resulting in a reduced demand for oxygen. Simultaneously, oxygen from the air enters the reaction solution progressively due to stirring, leading to an increase in dissolved oxygen content in the solution.

Although light is not directly involved in the Fe(III)/sulfite process, relevant study has shown that light can promote the generation of free radicals in sulfur autoxidation systems [47]. In this study, xenon lamps were used to simulate natural light and explore the effect of light on the degradation of deltamethrin by the Fe(III)/sulfite system. From Figure 6, it can be observed that there was no significant advantage under light conditions within the first 3 min of the reaction. However, with the reaction prolonging from 5 to 30 min, the degradation efficiency under light conditions began to be better than that under non-light conditions, with a degradation rate increase of about 10%. This improvement can be attributed to the promoted reactions of photosensitive sulfite species. Furthermore, light can promote the decomposition of Fe(III)-sulfite complexes [40], which ultimately leads to the enhanced degradation of deltamethrin.

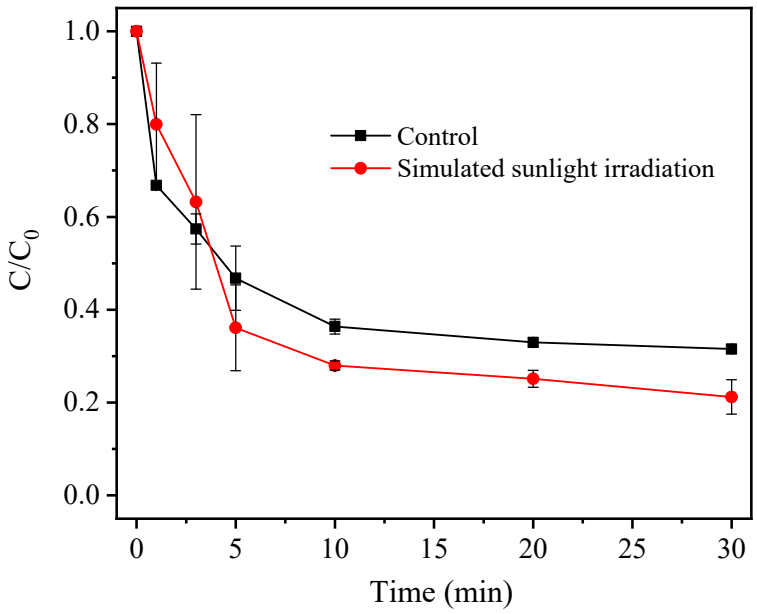

Figure 6. The effect of light on the degradation of deltamethrin. Condition: $[Deltamethrin]_0$ = 30 μg/L, $[Fe(III)]_0$ = 100 μM, $[HSO_3^-]_0$ = 1 mM, pH = 4 ± 0.2. The error bars represent the standard deviations.

3.5. Identification of the Radicals

To gain insights into the mechanism of the Fe(III)/sulfite system, EtOH and TBA were selected as radical scavengers. EtOH is effective for quenching both $SO_4^{\bullet-}$ and $HO^{\bullet}$, while TBA is usually considered more effective at quenching $HO^{\bullet}$ than $SO_4^{\bullet-}$ [48,49]. As shown in Figure 7a, the removal of deltamethrin decreased from 69.5% to 53% with

the addition of EtOH (1.2 mM) and TBA (1.2 mM), respectively. This indicated that $HO^{\bullet}$ more than $SO_4^{\bullet-}$ may take part in the reaction, and $HO^{\bullet}$ was the dominant oxidant. The potential free radicals in the Fe(III)/sulfite system after a 5 min reaction were also measured by EPR spectrum with the addition of DMPO. Figure 7b shows that only typical signals of DMPO-$HO^{\bullet}$ adduct were gained in both control sample and the TBA-added sample, further confirming the presence of $HO^{\bullet}$ in the Fe(III)/sulfite system. The typical signals of DMPO-$SO_4^{\bullet-}$ adduct was not found in either sample. This absence may be attributed to the limited generation of $SO_4^{\bullet-}$ and rapid conversion of $SO_4^{\bullet-}$ to $HO^{\bullet}$.

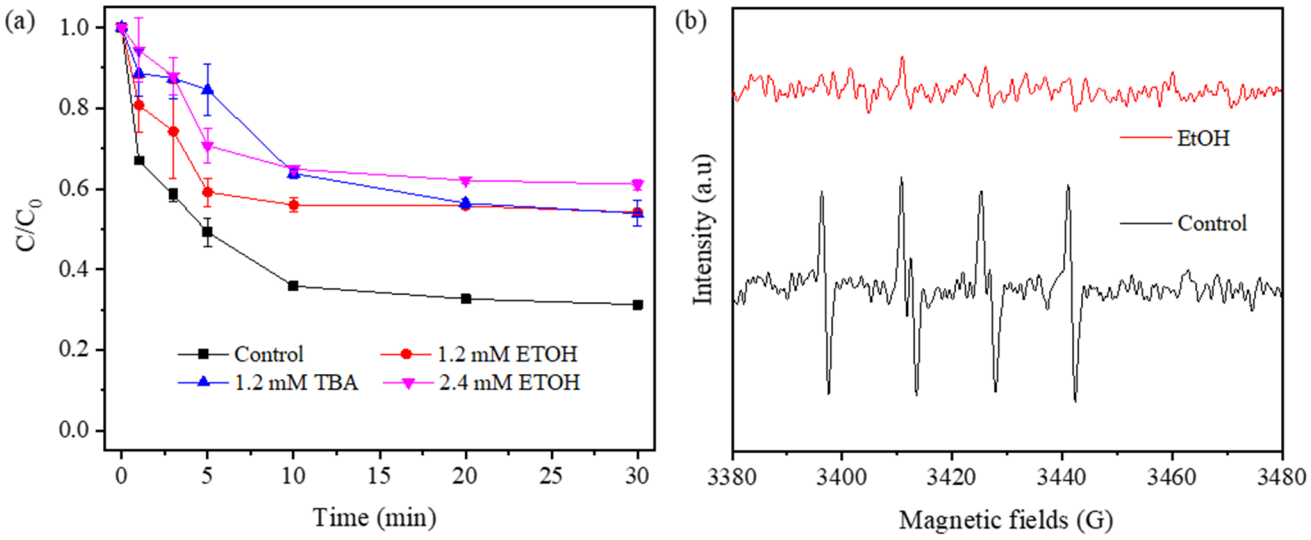

Figure 7. Effect of EtOH and TBA on deltamethrin removal by the Fe(III)/sulfite system (**a**) and the EPR spectra obtained from the Fe(III)/sulfite system with the addition of DMPO (**b**). Condition: $[Deltamethrin]_0$ = 30 μg/L, $[Fe(III)]_0$ = 100 μM, $[HSO_3^-]_0$ = 1 mM, pH = 4 ± 0.2. The error bars represent the standard deviations.

3.6. Deltamethrin Degradation Pathways

The geometric optimization and NBO charge calculations of deltamethrin molecules were conducted using the B3LYP and M06 methods within the density functional theory framework, employing the 6-31G+ (d, p) basis set (Figure 8). The optimized molecular structure of deltamethrin is illustrated in Figure S2 in Supplementary Materials, and the NBO charge calculation results are presented in Table S1 in Supplementary Materials. Notably, the findings indicate that bond-breaking reactions are prone to occur at C16-O21 and C31-O36, while C38 and C39 are inclined towards substitution reactions.

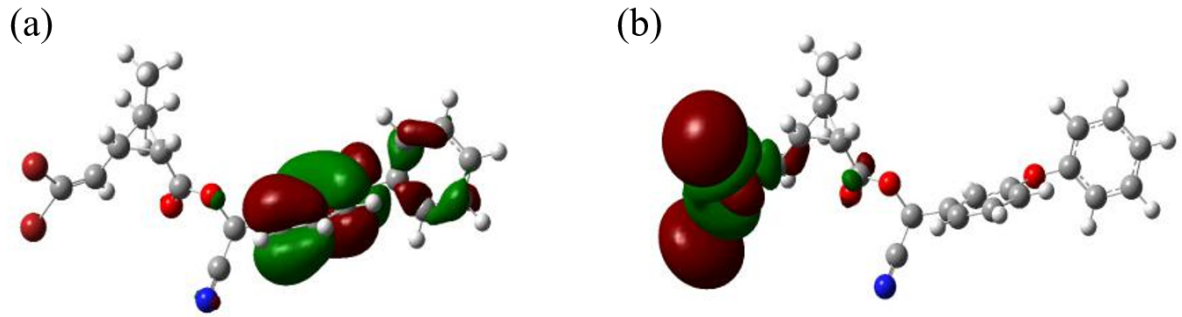

Figure 8. Homo (**a**) and Lumo (**b**) orbital diagrams of deltamethrin molecules.

As highlighted in Table S2, it is evident that the results derived from both the M06 and B3LYP methods exhibit substantial similarity. It is essential to note that a higher Fukui function value corresponds to an increased susceptibility of a specific point to attack. In

the case of the deltamethrin molecule, the most vulnerable sites are Br18 and Br19, while those susceptible to attack by HO• are C14, C27, C31, and O36. It is of particular interest that the bond between C31 and O36 is susceptible to breakage through free radical attack. The potential degradation pathways of deltamethrin were hypothesized by integrating the NBO charge calculations with the outcomes of Fukui function calculations. Firstly, C16-O21 is attacked by free radicals in a bond-breaking reaction. The resulting product, P1, may further undergo hydrolysis, giving rise to P3, as Cyano is unstable under acidic conditions and susceptible to hydrolysis. Secondly, free radicals attack C31-O36, leading to a bond-breaking reaction and yielding P4 and P5. P4 may undergo further oxidation by -OH during degradation, leading to another bond-breaking reaction at C16-O21, producing P6. Thirdly, radicals attack one or more of C14, C27, C38, C39, undergoing a substitution reaction and resulting in P7, P8, P9, P10, P11, P12, P13, P14, and P15.

To further clarify the degradation pathway of deltamethrin, the degradation products after 30 min were analyzed by GC-MS. The results are presented in Table S3 (Supplementary Materials). Only P1 and P3 were detected in the degradation products at 30 min, which aligns with the products in step 1. Notably, P4 was not detected after 30 min of reaction, while P1 was detected. This suggests that C16-O21 is more susceptible to fracture compared to C31-O36, which deviates slightly from the results obtained from NBO charge calculations. The proposed pathways of deltamethrin in the Fe(III)/sulfite system are shown in Figure 9.

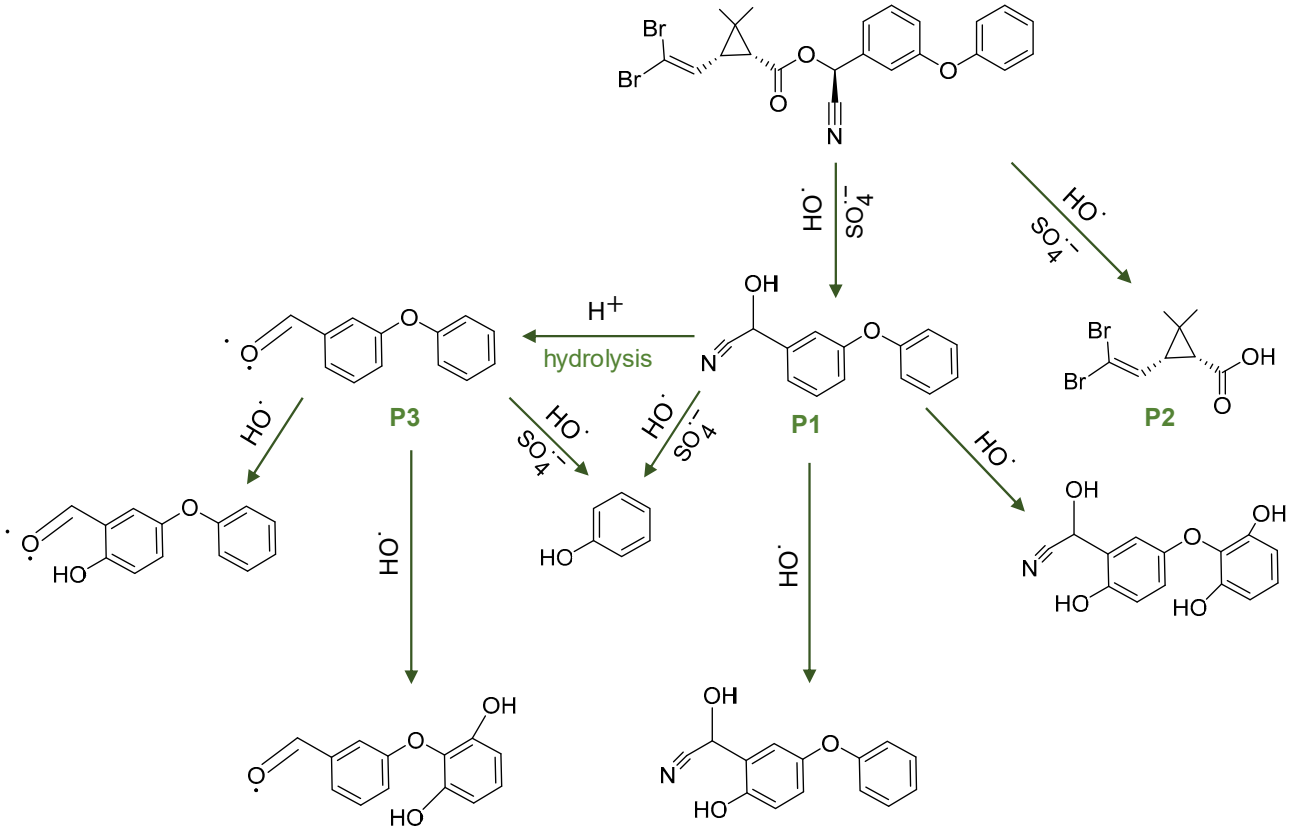

Figure 9. Proposed pathways of deltamethrin in the Fe(III)/sulfite system.

3.7. The Degradation Efficiency in Secondary Effluent

Figure 5a,b indicate that the degradation of deltamethrin would be inhibited by HA and HCO_3^-, which is widely present in nature water matrices. Therefore, the degradation efficiency of pollutants by Fe(III)/sulfite in a secondary effluent was further evaluated. The characteristics of the secondary effluent used in this experiment are detailed in Table S4 (Supplementary Materials). As depicted in Figure 10, the degradation rate of deltamethrin

was 47.3%, representing a decrease of 22.4% compared with the control sample. This reduction indicates the presence of free radical inhibitors in the secondary effluent, which could compete with deltamethrin and react with free radicals. However, despite this partial inhibition, the Fe(III)/sulfite system still demonstrated a noticeable degradation performance. This indicates that the Fe(III)/sulfite system could be applied in the treatment of refractory organics during the advanced stages of sewage treatment.

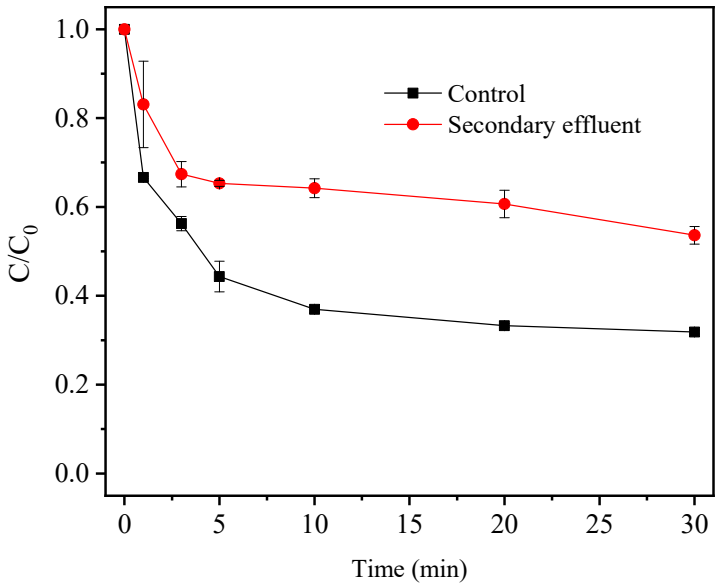

Figure 10. The degradation efficiency of deltamethrin in a secondary effluent. Condition: $[Deltamethrin]_0$ = 30 μg/L, $[Fe(III)]_0$ = 100 μM, $[HSO_3^-]_0$ = 1 mM, pH = 4 ± 0.2. The error bars represent the standard deviations.

As shown in Figure S5 in Supplementary Materials, the COD of the solution reduced by 40%, meeting the first-class standard of A in the "Discharge Standard of Pollutants for Municipal Wastewater Treatment Plant"[50]. However, with the development of urban areas, the existing treatment process is no longer sufficient to meet the growing demand and requires retrofitting. Therefore, it is worth considering the addition of an advanced treatment process at the end to facilitate the degradation of micropollutants and achieve a substantial reduction in the COD value of the effluent. The utilization of transition metal activation of sulfite in the water treatment process is easily attainable. This is due to the fact that during water treatment, flocculants such as iron salts are added in the flocculation stage. These iron salts can subsequently serve as a catalyst for the sulfur (IV) auto-oxidation system, producing $HO^•$ and $SO_4^{•-}$.

3.8. Control of BrO_3^- Formation

BrO_3^- is a common inorganic byproduct with strong carcinogenicity and genetic toxicity in drinking water treatment and was classified as a potential carcinogen at the level of 2B by many international research institutions [51]. In traditional advanced oxidation processes, it has been reported that Br^- undergoes a series of transformation and is oxidized to BrO_3^- by $SO_4^{•-}$ and $HO^•$. During the ozonation disinfection process, ozone promotes the conversion of Br^- to BrO_3^-, and the formation of BrO_3^- is enhanced by increased ozone concentration and reaction time [52]. Additionally, research has shown that the reaction between Br^- and $SO_4^{•-}$ can form BrO_3^- in the Co(II)/PMS system [53]. Therefore, it is important to evaluate the formation of BrO_3^- during the degradation of organic pollutants by AOPs. The change of Br^- concentration and the formation of BrO_3^- during the degradation of deltamethrin by the Fe(III)/sulfite system in the presence of Br^- (20 μM) were studied. As shown in Figure S6, there was no production of BrO_3^- during the reaction process, and the content of Br^- remained relatively unchanged. This could be attributed

to the strong reductive properties of sulfite, which rapidly consumes bromine-containing oxidants and inhibits the generation of BrO_3^-. Thus, the proposed Fe(III)/sulfite system would be a favorable choice for the degradation of organic pollutants in the presence of Br^-, allowing for effective control of BrO_3^-, as opposed to traditional AOPs.

4. Conclusions

In this study, a high degradation efficiency of deltamethrin was achieved using the sulfur autoxidation system of Fe(III)/sulfite. It was observed that pH levels ranging from 3 to 7 hindered the degradation of deltamethrin. However, increasing the Fe(III) concentration from 60 to 100 μM and sulfite concentration from 0.25 to 1.5 mM enhanced the degradation of deltamethrin. Both bicarbonate and HA were found to inhibit the degradation of deltamethrin in this system, with the removal of deltamethrin decreasing by 22% in the absence of oxygen. $HO^•$ and $SO_4^{•-}$ participated in the oxidation of deltamethrin, with $HO^•$ being the dominant free radical in the Fe(III)/sulfite system. Additionally, density functional theory analysis revealed that the bond-breaking reaction between C16 and O21 in deltamethrin easily occurred, and this degradation pathway was confirmed through GC-MS analysis. Noticeable degradation performance was achieved by Fe(III)/sulfite during secondary effluent treatment, and the Fe(III)/sulfite system exhibited excellent performance in the formation of BrO_3^- in the presence of Br^-.

Supplementary Materials: The following supporting information can be downloaded at https://www.mdpi.com/article/10.3390/w16010008/s1: Text S1. Method for the incident light intensity measure. Figure S1. Variation of pH values in systems under different concentrations of HCO_3^-; Figure S2. Molecular structure diagram of deltamethrin; Figure S3. Bitmap of vulnerable points of deltamethrin molecules; Figure S4. Inferred degradation pathway of deltamethrin; Figure S5. Variation of COD concentration during reaction in secondary effluent; Figure S6. The change of Br^- and formation of BrO_3^- during the degradation of deltamethrin by Fe(III)/sulfite system in the presence of Br^- (20 μM); Table S1. NBO charge calculation of deltamethrin molecules; Table S2. Fukui function table of deltamethrin molecules; Table S3. Degradation products detected by GC-MS; Table S4. The characteristics of the secondary effluent used in this experiment. References [54–56] are cited in the supplementary materials.

Author Contributions: Experimental design, P.X. and L.Y.; methodology, J.D. and Y.W.; investigation, Y.W. and L.Y.; writing—review and revision, Y.W., J.D. and H.W.; visualization, L.Y. and Z.W.; formal analysis, F.S. and Y.P.; acquisition of funding, Z.W. and P.X. All authors have read and agreed to the published version of the manuscript.

Funding: The work was funded by the Natural Science Foundation of China (No. 52070081), the special fund of The Yangtze River Joint Research Phase II Program (2022LHYJ02050403), Science, Technology and Innovation Commission of Shenzhen Municipality (Grant No. JSGG20201103094600001), PowerChina technology project (No. DJ-HXGG-2022-09), PowerChina Eco-environmental Group Co., Ltd. technology project (No. KYZB2022Z003), National Key Research and Development Program of China (2022YFC3203500).

Data Availability Statement: Data are contained within the article.

Conflicts of Interest: Author Y.W., F.S., H. W., and Y.P. was employed by the company Power China Eco-Environmental Group Co., Ltd. The remaining authors declare that the research was conducted in the absence of any commercial or financial relation-ships that could be construed as a potential conflict of interest.

References

1. Felten, V.; Toumi, H.; Masfaraud, J.-F.; Billoir, E.; Camara, B.I.; Férard, J.-F. Microplastics enhance Daphnia magna sensitivity to the pyrethroid insecticide deltamethrin: Effects on life history traits. *Sci. Total Environ.* **2020**, *714*, 136567. [CrossRef] [PubMed]
2. Lu, Q.; Sun, Y.; Ares, I.; Anadón, A.; Martínez, M.; Martínez-Larrañaga, M.-R.; Yuan, Z.; Wang, X.; Martínez, M.-A. Deltamethrin toxicity: A review of oxidative stress and metabolism. *Environ. Res.* **2019**, *170*, 260–281. [CrossRef] [PubMed]
3. Chernistry, P. Cypermethrin and Deltamethrin Insecticides in Male Rats. *J. Pharmacol. Toxicol.* **2012**, *7*, 312–321. [CrossRef]

4. Hassan, A.; Youssef, A.; Priecel, P. Removal of deltamethrin insecticide over highly porous activated carbon prepared from pistachio nutshells. *Carbon Lett.* **2013**, *14*, 234–242. [CrossRef]
5. Lafi, W.K.; Al-Qodah, Z. Combined advanced oxidation and biological treatment processes for the removal of pesticides from aqueous solutions. *J. Hazard Mater.* **2006**, *137*, 489–497. [CrossRef] [PubMed]
6. Giannakis, S.; Lin, K.-Y.A.; Ghanbari, F. A review of the recent advances on the treatment of industrial wastewaters by Sulfate Radical-based Advanced Oxidation Processes (SR-AOPs). *Chem. Eng. J.* **2021**, *406*, 127083. [CrossRef]
7. Wang, Z.; Jiang, J.; Pang, S.; Zhou, Y.; Guan, C.; Gao, Y.; Li, J.; Yang, Y.; Qiu, W.; Jiang, C. Is sulfate radical really generated from peroxydisulfate activated by iron (II) for environmental decontamination? *Environ. Sci. Technol.* **2018**, *52*, 11276–11284. [CrossRef] [PubMed]
8. Lin, Q.; Deng, Y. Is sulfate radical a ROS? *Environ. Sci. Technol.* **2021**, *55*, 15010–15012. [CrossRef]
9. Xu, Y.; Che, T.; Li, Y.; Fang, C.; Dai, Z.; Li, H.; Xu, L.; Hu, F. Remediation of polycyclic aromatic hydrocarbons by sulfate radical advanced oxidation: Evaluation of efficiency and ecological impact. *Ecotoxicol. Environ. Saf.* **2021**, *223*, 112594. [CrossRef]
10. Ushani, U.; Lu, X.; Wang, J.; Zhang, Z.; Dai, J.; Tan, Y.; Wang, S.; Li, W.; Niu, C.; Cai, T. Sulfate radicals-based advanced oxidation technology in various environmental remediation: A state-of-the–art review. *Chem. Eng. J.* **2020**, *402*, 126232. [CrossRef]
11. Zhang, J.; Zhu, L.; Shi, Z.; Gao, Y. Rapid removal of organic pollutants by activation sulfite with ferrate. *Chemosphere* **2017**, *186*, 576–579. [CrossRef] [PubMed]
12. Huang, L.-Z.; Wei, X.; Gao, E.; Zhang, C.; Hu, X.-M.; Chen, Y.; Liu, Z.; Finck, N.; Luetzenkirchen, J.; Dionysiou, D.D. Single Fe atoms confined in two-dimensional MoS_2 for sulfite activation: A biomimetic approach towards efficient radical generation. *Appl. Catal. B* **2020**, *268*, 118459. [CrossRef]
13. Chen, H.; Lin, T.; Wang, P.; Zhang, X.; Jiang, F.; Wang, Y. Novel solar/sulfite advanced oxidation process for carbamazepine degradation: Radical chemistry, transformation pathways, influence on disinfection byproducts and toxic changes. *Chem. Eng. J.* **2023**, *451*, 138634. [CrossRef]
14. Tong, R.; Fu, R.; Yang, Z.; Jiang, Y.; Jiang, K.; Sun, X. Efficient degradation of sulfachloropyridazine by sulfite activation with CuO-Al_2O_3 composites under neutral pH conditions: Radical and non-radical. *J. Environ. Chem. Eng.* **2022**, *10*, 107276. [CrossRef]
15. Cong, Y.; Shen, L.; Wang, B.; Cao, J.; Pan, Z.; Wang, Z.; Wang, K.; Li, Q.; Li, X. Efficient removal of Cr (VI) at alkaline pHs by sulfite/iodide/UV: Mechanism and modeling. *Water Res.* **2022**, *222*, 118919. [CrossRef] [PubMed]
16. Dong, Q.; Dong, H.; Li, Y.; Xiao, J.; Xiang, S.; Hou, X.; Chu, D. Degradation of sulfamethazine in water by sulfite activated with zero-valent Fe-Cu bimetallic nanoparticles. *J. Hazard. Mater.* **2022**, *431*, 128601. [CrossRef] [PubMed]
17. Zhou, A.; Liu, H.; Varrone, C.; Shyryn, A.; Defemur, Z.; Wang, S.; Liu, W.; Yue, X. New insight into waste activated sludge acetogenesis triggered by coupling sulfite/ferrate oxidation with sulfate reduction-mediated syntrophic consortia. *Chem. Eng. J.* **2020**, *400*, 125885. [CrossRef]
18. Duan, S.; Hou, P.; Yuan, X.; Stanić, M.H.; Qiang, Z.; Dong, H. Homogeneous activation of bisulfite by transition metals for micro-pollutant degradation: Mn (VII) versus Cr (VI). *Chem. Eng. J.* **2020**, *394*, 124814. [CrossRef]
19. Wang, H.; Wang, S.; Liu, Y.; Fu, Y.; Wu, P.; Zhou, G. Degradation of diclofenac by Fe (II)-activated bisulfite: Kinetics, mechanism and transformation products. *Chemosphere* **2019**, *237*, 124518. [CrossRef]
20. Chen, L.; Peng, X.; Liu, J.; Li, J.; Wu, F. Decolorization of orange II in aqueous solution by an Fe (II)/sulfite system: Replacement of persulfate. *Ind. Eng. Chem. Res.* **2012**, *51*, 13632–13638. [CrossRef]
21. Grgićc, I.; Pozničc, M.; Bizjak, M. S (IV) autoxidation in atmospheric liquid water: The role of Fe (II) and the effect of oxalate. *J. Atmos. Chem.* **1999**, *33*, 89–102. [CrossRef]
22. Neta, P.; Huie, R.E.; Ross, A.B. Rate constants for reactions of inorganic radicals in aqueous solution. *J. Phys. Chem. Ref. Data* **1988**, *17*, 1027–1284. [CrossRef]
23. Warneck, P.; Ziajka, J. Reaction Mechanism of the Iron (III)-Catalyzed Autoxidation of Bisulfite in Aqueous Solution: Steady State Description for Benzene as Radical Scavenger. *Berichte Bunsenges. Phys. Chem.* **1995**, *99*, 59–65. [CrossRef]
24. Xie, P.; Zhang, L.; Wang, J.; Zou, Y.; Wang, S.; Yue, S.; Wang, Z.; Ma, J. Transformation of tetrabromobisphenol a in the iron ions-catalyzed auto-oxidation of HSO_3^{2-}/SO_3^{2-} process. *Sep. Purif. Technol.* **2020**, *235*, 116197. [CrossRef]
25. Yermakov, A.N.; Poskrebyshev, G.A.; Stoliarov, S.I. Temperature dependence of the branching ratio of SO_5^- radicals self-reaction in aqueous solution. *J. Phys. Chem.* **1996**, *100*, 3557–3560. [CrossRef]
26. Brandt, C.; Van Eldik, R. Transition metal-catalyzed oxidation of sulfur (IV) oxides. Atmospheric-relevant processes and mechanisms. *Chem. Rev.* **1995**, *95*, 119–190. [CrossRef]
27. Zhang, Y.; Zhou, J.; Li, C.; Guo, S.; Wang, G. Reaction kinetics and mechanism of iron (II)-induced catalytic oxidation of sulfur (IV) during wet desulfurization. *Ind. Eng. Chem. Res.* **2012**, *51*, 1158–1165. [CrossRef]
28. Kuo, D.T.; Kirk, D.W.; Jia, C.Q. The chemistry of aqueous S (IV)-Fe-O_2 system: State of the art. *J. Sulfur Chem.* **2006**, *27*, 461–530. [CrossRef]
29. Chen, X.; Miao, W.; Yang, Y.; Hao, S.; Mao, S. Aeration-assisted sulfite activation with ferrous for enhanced chloramphenicol degradation. *Chemosphere* **2020**, *238*, 124599. [CrossRef]
30. Ren, Y.; Chu, Y.; Li, N.; Lai, B.; Zhang, W.; Liu, C.; Li, J. A critical review of environmental remediation via iron-mediated sulfite advanced oxidation processes. *Chem. Eng. J.* **2023**, *455*, 140859. [CrossRef]
31. Zhang, L.; Chen, L.; Xiao, M.; Zhang, L.; Wu, F.; Ge, L. Enhanced Decolorization of Orange II Solutions by the Fe(II)–Sulfite System under Xenon Lamp Irradiation. *Ind. Eng. Chem. Res.* **2013**, *52*, 10089–10094. [CrossRef]

32. Wu, S.; Shen, L.; Lin, Y.; Yin, K.; Yang, C. Sulfite-based advanced oxidation and reduction processes for water treatment. *Chem. Eng. J.* **2021**, *414*, 128872. [CrossRef]
33. Fang, J.-Y.; Shang, C. Bromate formation from bromide oxidation by the UV/persulfate process. *Environ. Sci. Technol.* **2012**, *46*, 8976–8983. [CrossRef] [PubMed]
34. Wu, H.; Gao, X.; Wu, M.; Zhu, Y.; Xiong, R.; Ye, S. The efficiency and risk to groundwater of constructed wetland system for domestic sewage treatment-A case study in Xiantao, China. *J. Clean. Prod.* **2020**, *277*, 123384. [CrossRef]
35. Tozer, D.J.; De Proft, F. Modeling temporary anions in density functional theory: Calculation of the Fukui function. *J. Chem. Phys.* **2007**, *127*, 034108. [CrossRef] [PubMed]
36. Du, J.; Guo, W.; Wang, H.; Yin, R.; Zheng, H.; Feng, X.; Che, D.; Ren, N. Hydroxyl radical dominated degradation of aquatic sulfamethoxazole by Fe^0/bisulfite/O_2: Kinetics, mechanisms, and pathways. *Water Res.* **2018**, *138*, 323–332. [CrossRef] [PubMed]
37. Lee, C.; Keenan, C.R.; Sedlak, D.L. Polyoxometalate-enhanced oxidation of organic compounds by nanoparticulate zero-valent iron and ferrous ion in the presence of oxygen. *Environ. Sci. Technol.* **2008**, *42*, 4921–4926. [CrossRef]
38. Zhou, T.; Li, Y.; Ji, J.; Wong, F.-S.; Lu, X. Oxidation of 4-chlorophenol in a heterogeneous zero valent iron/H_2O_2 Fenton-like system: Kinetic, pathway and effect factors. *Sep. Purif. Technol.* **2008**, *62*, 551–558. [CrossRef]
39. Zhang, H.; Zhang, Y.; Hou, Z.; Wang, X.; Wang, J.; Lu, Z.; Zhao, X.; Sun, F.; Pan, H. Biodegradation potential of deltamethrin by the Bacillus cereus strain Y1 in both culture and contaminated soil. *Int. Biodeterior. Biodegrad.* **2016**, *106*, 53–59. [CrossRef]
40. Xie, P.; Zhang, L.; Chen, J.; Ding, J.; Wan, Y.; Wang, S.; Wang, Z.; Zhou, A.; Ma, J. Enhanced degradation of organic contaminants by zero-valent iron/sulfite process under simulated sunlight irradiation. *Water Res.* **2019**, *149*, 169–178. [CrossRef]
41. Cao, Y.; Qiu, W.; Li, J.; Jiang, J.; Pang, S. Review on UV/sulfite process for water and wastewater treatments in the presence or absence of O_2. *Sci. Total Environ.* **2021**, *765*, 142762. [CrossRef] [PubMed]
42. Liu, Z.; Guo, Y.; Shang, R.; Fang, Z.; Wu, F.; Wang, Z. A triple system of Fe (III)/sulfite/persulfate: Decolorization and mineralization of reactive Brilliant Red X-3B in aqueous solution at near-neutral pH values. *J. Taiwan Inst. Chem. Eng.* **2016**, *68*, 162–168. [CrossRef]
43. Deng, W.; Zhao, H.; Pan, F.; Feng, X.; Jung, B.; Abdel-Wahab, A.; Batchelor, B.; Li, Y. Visible-light-driven photocatalytic degradation of organic water pollutants promoted by sulfite addition. *Environ. Sci. Technol.* **2017**, *51*, 13372–13379. [CrossRef] [PubMed]
44. Gao, Y.; Fan, W.; Zhang, Z.; Zhou, Y.; Zeng, Z.; Yan, K.; Ma, J.; Hanna, K. Transformation mechanisms of iopamidol by iron/sulfite systems: Involvement of multiple reactive species and efficiency in real water. *J. Hazard. Mater.* **2022**, *426*, 128114. [CrossRef] [PubMed]
45. Ren, Z.; Bergmann, U.; Leiviskä, T. Reductive degradation of perfluorooctanoic acid in complex water matrices by using the UV/sulfite process. *Water Res.* **2021**, *205*, 117676. [CrossRef] [PubMed]
46. Jiang, B.; Liu, Y.; Zheng, J.; Tan, M.; Wang, Z.; Wu, M. Synergetic transformations of multiple pollutants driven by Cr (VI)–sulfite reactions. *Environ. Sci. Technol.* **2015**, *49*, 12363–12371. [CrossRef] [PubMed]
47. Xu, J.; Ding, W.; Wu, F.; Mailhot, G.; Zhou, D.; Hanna, K. Rapid catalytic oxidation of arsenite to arsenate in an iron (III)/sulfite system under visible light. *Appl. Catal. B* **2016**, *186*, 56–61. [CrossRef]
48. Zhu, C.; Zhu, F.; Dionysiou, D.D.; Zhou, D.; Fang, G.; Gao, J. Contribution of alcohol radicals to contaminant degradation in quenching studies of persulfate activation process. *Water Res.* **2018**, *139*, 66–73. [CrossRef]
49. Tan, C.; Jian, X.; Dong, Y.; Lu, X.; Liu, X.; Xiang, H.; Cui, X.; Deng, J.; Gao, H. Activation of peroxymonosulfate by a novel EGCE@ Fe_3O_4 nanocomposite: Free radical reactions and implication for the degradation of sulfadiazine. *Chem. Eng. J.* **2019**, *359*, 594–603. [CrossRef]
50. *GB18918-2002*; Discharge Standard of Pollutants for Municipal Wastewater Treatment Plant. Ministry of Ecology and Environment, The People's Republic of China: Beijing, China, 2003.
51. Moore, M.M.; Chen, T. Mutagenicity of bromate: Implications for cancer risk assessment. *Toxicology* **2006**, *221*, 190–196. [CrossRef]
52. Pinkernell, U.; Von Gunten, U. Bromate minimization during ozonation: Mechanistic considerations. *Environ. Sci. Technol.* **2001**, *35*, 2525–2531. [CrossRef] [PubMed]
53. Liu, K.; Lu, J.; Ji, Y. Formation of brominated disinfection by-products and bromate in cobalt catalyzed peroxymonosulfate oxidation of phenol. *Water Res.* **2015**, *84*, 1–7. [CrossRef] [PubMed]
54. He, J.; Zhang, Y.; Guo, Y.; Rhodes, G.; Yeom, J.; Li, H.; Zhang, W. Photocatalytic degradation of cephalexin by ZnO nanowires under simulated sunlight: Kinetics, influencing factors, and mechanisms. *Environ. Int.* **2019**, *132*, 105105. [CrossRef] [PubMed]
55. Birkigt, J.; Gilevska, T.; Ricken, B.; Richnow, H.H.; Vione, D.; Corvini, P.F.X.; Nijenhuis, I.; Cichocka, D. Carbon stable isotope fractionation of sulfamethoxazole during biodegradation by Microbacterium sp. strain BR1 and upon direct photolysis. *Environ. Sci. Tech.* **2015**, *49*, 6029–6036. [CrossRef] [PubMed]
56. Méndez-Díaz, J.D.; Shimabuku, K.K.; Ma, J.; Enumah, Z.O.; Pignatello, J.J.; Mitch, W.A.; Dodd, M.C. Sunlight-driven photochemical halogenation of dissolved organic matter in seawater: A natural abiotic source of organobromine and organoiodine. *Environ. Sci. Tech.* **2014**, *48*, 7418–7427. [CrossRef]